LANGMUIR Article
Cite This: Langmuir 2019, 35, 6540−6549
pubs.acs.org/Langmuir

Effect of Carboxylic Acid on the Wetting Properties of a Model Water−Octane−Silica System

Wenjing Guo and Jeffrey R. Errington*

Department of Chemical and Biological Engineering, University at Buffalo, Buffalo, New York 14260-4200, United States

ABSTRACT: Monte Carlo simulations are employed to determine the effects of acetic acid on the wetting properties of a model water−octane−silica system. We first compute the bulk liquid−vapor saturation properties of pure acetic acid and subsequently explore the bulk liquid−liquid saturation properties of the ternary water−octane−acid system. We introduce an expanded ensemble approach to compute the coexistence properties of the ternary system. An interface potential approach is then used to capture the evolution of the wetting properties of the water−octane−silica system upon the addition of acetic acid. We track the change in the octane−water interfacial tension and the contact angle of water droplet on a silica substrate in a mother octane fluid over a range of acetic acid activities. The structure of the fluid, including the partitioning of acetic acid within the interfacial system, is also considered at several state points. We observe that acetic acid has a strong tendency to adsorb at the octane−water interface, resulting in a reduction in the octane−water interfacial tension. The response of the contact angle is more sensitive to the temperature and the hydrophilicity of the silica substrate.

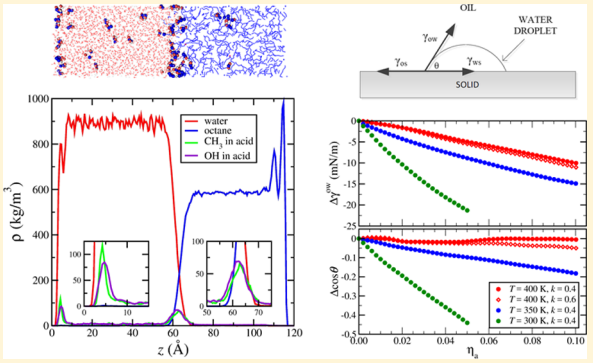

INTRODUCTION

The wetting characteristics of an oil reservoir play an important role in the oil recovery process.[1] Many enhanced oil recovery (EOR) strategies have been designed to modify wetting properties by altering the microscopic environment within the oil reservoir. The well environment is characterized by porous rock surrounded by oil- and water-based liquids.[2] The relative preference that the rock exhibits for the oil and water phases under equilibrium conditions has a significant impact on the extent to which oil can be recovered from the well.[3] If oil preferentially adsorbs on the rock surface (oil-wet system), then the oil phase will dominate the rock−fluid interfacial region. In such a case, the smallest of pores are likely to exclude water completely, whereas larger pores may accommodate some water within the pore center. If water preferentially wets the rock surface (water-wet system), the scenario is reversed and oil is excluded from the rock pores.

Natural (clean) mineral surfaces characteristic of oil reservoirs generally exhibit water-wet interfacial properties.[4] However, the history of the rock surface (e.g., previous contact with oil) can significantly alter this picture. Over long periods of time, hydrocarbons can displace water within rock pores, as the wetting preference evolves from water-wet to oil-wet.[5−9] Many have speculated that the heavy asphaltene fractions of crude oil are responsible for this wetting alteration.[10−12] It has been suggested that during the aging process, charged components within the asphaltene fraction, such as acids and bases, adsorb onto the rock surface, thereby changing the surface chemistry of the rock. The design of EOR strategies could be aided significantly by a better fundamental understanding of how surface active polar organic molecules influence the wetting properties of rock−water−oil systems.

A number of experimental studies have established the role of carboxylic acids in modifying the interfacial properties of calcite.[8,13−19] For example, Wu et al.[18] demonstrated the effect of adsorbed carboxylic acid on the contact angle of water at a calcite surface. They observed that the change in the contact angle increased with an increase in the hydrophobicity of the carboxylic acid, which they explained in terms of a shift in the effective surface energy of calcite. There have been relatively few molecular simulation studies devoted to this topic,[20−23] and the approach pursued within these studies has generally been phenomenological in nature.

Zhong et al.[4] utilized molecular dynamics simulation to study the adsorption of organic molecules onto minerals from a microscopic perspective. More specifically, they studied a process in which organic molecules migrate through a water film and adsorb onto a silica substrate. They considered how components with varying polarity, including *n*-decane, methyl benzene, pyridine, and acetic acid, partition between the silica−water interface and the water−vapor interface. The group also explored the dynamics and energetics associated with the adsorption process. Their results showed that apolar molecules (*n*-decane, methyl benzene) are preferentially excluded from the substrate, whereas polar molecules (pyridine, acetic acid) are preferentially adsorbed at the silica−water interface. The study supports the important role

Received: February 7, 2019
Revised: April 29, 2019
Published: April 30, 2019

DOI: 10.1021/acs.langmuir.9b00393
Langmuir 2019, 35, 6540−6549

polarity plays in the manner in which molecules partition within interfacial systems.

Jiménez-Ángeles and Firoozabadi recently employed molecular dynamics simulation to study the wettability of an alkane−water mixture at a muscovite mica substrate.[24,25] They examined the variation of the liquid−liquid interfacial tension and the contact angle of a *n*-decane droplet at a mica substrate in a mother aqueous phase with salt concentration. The authors observed a decrease in contact angle with increasing salt concentration and linked this to the manner in which water and salt organize at the substrate. They also considered the impact of a surfactant on the wetting behavior. They report that the presence of a surfactant leads to a decrease in liquid−liquid interfacial tension and increase in the contact angle.

Jiang et al. studied the related silica−water−carbon dioxide system.[26] The authors extended the phantom wall method[27,28] developed by Leroy and Müller-Plathe to accommodate systems at fluid−fluid equilibrium. The method was used to compute the contact angle of a water droplet on a silica surface in a mother supercritical carbon dioxide phase. Results for the contact angle were consistent with experimental data.

Headen and Boek employed molecular simulation to study the adsorption of a representative asphaltene molecule at a calcite surface.[23] More specifically, they computed the potential of mean force associated with the asphaltene molecule in the vicinity of the calcite surface in an effective dielectric medium. They quantified the degree of attraction between the asphaltene and the calcite substrate.

The accumulation of carboxylic acids at the water−hydrocarbon interface has been studied both theoretically and experimentally.[29−31] These studies show that carboxylic acids act as a surfactant at hydrocarbon−water interfaces and reduce the interfacial tension. For example, Holte et al.[29] used molecular simulation to detail the structure of lauric acid at water−*n*-hexane and water−carbon tetrachloride interfaces. They considered the manner in which lauric acid organizes and orients at the water−hydrocarbon interface. They also examined how the width of the interfacial region varies with increasing surfactant concentration.

In this work, we use Monte Carlo (MC) simulation to study the impact of a polar organic compound on the wetting properties of a model rock−water−oil system. More specifically, we examine a system consisting of a water-rich liquid phase and an *n*-octane-rich liquid phase in the vicinity of a silica substrate. Acetic acid is introduced as a representative polar organic molecule. We consider the impact of acetic acid on measures of wettability, such as the liquid−liquid interfacial tension and contact angle of a water-rich droplet at a silica substrate in a mother octane-rich liquid phase. We also examine how acetic acid partitions between the liquid−liquid and mineral−fluid interfaces. Our results provide quantitative relationships between the concentration of acetic acid (both in the bulk and at the surface) and the interfacial tension and water contact angle. The acetic acid accumulates at the liquid−liquid interface and exhibits surfactant-like characteristics. An increase in acetic acid concentration results in a decrease in the interfacial tension. The response of the contact angle varies with temperature and the hydrophilicity of the substrate.

We begin by constructing bulk liquid−liquid saturation lines associated with the addition of acetic acid to the water−octane system at constant temperature and pressure. We then evaluate the evolution of the liquid−liquid interfacial tension and water contact angle along these bulk saturation curves. Calculation of these properties requires modest extensions of methods previously introduced by our group.[32−34] We employ an expanded ensemble (EE) MC method to trace bulk saturation curves over a range of acetic acid activities. An interface potential approach is used to compute the wetting properties of interest.

The article is organized as follows. In the next section, we discuss the simulation methods used to compute bulk and interfacial properties. We then discuss the molecular models employed and provide relevant details for the simulations performed in this work. Next, we present and discuss our simulation results. Finally, we provide concluding remarks.

METHODS

Bulk Saturation Properties. We begin by describing the method employed to compute bulk coexistence properties for the ternary water−octane−acetic acid system. The general method employed here is detailed in a recent study from our group,[35] and therefore we restrict our focus to new elements related to the introduction of acetic acid. At sufficiently high pressure and relatively low acetic acid activity, the system separates into water-rich and octane-rich liquid phases. Here, we are interested in the properties of these coexisting phases over a range of acetic acid activity at a given temperature and pressure. We work within a grand canonical (GC) ensemble in which the temperature, T, chemical potentials of the three species, μ_1, μ_2, μ_3, and volume, V are fixed and the particle numbers of the species, N_1, N_2, N_3 and energy, E fluctuate. In what follows, we use the inverse temperature, $\beta = 1/k_BT$ (k_B is Boltzmann's constant) and activities, $\xi_i = q_i e^{\beta\mu^i}$ (q_i represents the component of the molecular partition function of species i stemming from integration over momenta) to describe the temperature and chemical potentials, respectively. For convenience, the activities are often expressed in terms of an activity sum, $\chi = \xi_1 + \xi_2 + \xi_3$ and an activity fraction, $\eta_i = \xi_i/\chi$.

We work with the species water (w), *n*-octane (o), and acetic acid (a). Our aim is to deduce the relationship between the activities (ξ_w, ξ_o, ξ_a) for $\eta_a \in [0, 0.1]$ along a bulk liquid−liquid saturation line at specified T and pressure, p. Over this range of η_a, the concentration of acetic acid remains relatively low within both coexisting phases. The first point along this path, $\eta_a = \xi_a = 0.0$, corresponds to a binary water−octane system. In an earlier study,[35] we determined the saturation conditions for this binary mixture over a wide range of temperature and pressure. These data serve as reference points (ξ_w, ξ_o, 0.0) for the current study.

The task is to identify the activities (ξ_w, ξ_o, ξ_a) that satisfy the relationships

$$\Omega^w(\xi_w, \xi_o, \xi_a) = -\beta pV \tag{1}$$

$$\Omega^o(\xi_w, \xi_o, \xi_a) = -\beta pV \tag{2}$$

where β and p are the fixed inverse temperature and pressure and Ω^w and Ω^o are the grand potentials of the water-rich and octane-rich liquid phases, respectively. To accomplish this task, we establish a series of subensembles along the path of interest. Each subensemble is defined by a set of activities denoted $\lambda = (\xi_w, \xi_o, \xi_a)$. In practice, the subensembles are initially separated by a fixed difference in η_a. The goal is to establish the conditions λ^{sat} that satisfy eqs 1 and 2 for each subensemble. We initiate the calculation with an estimated λ^g for how λ varies along the saturation line. We then perform independent EE simulations to obtain the relative grand potentials Ω^w and Ω^o along the path. The absolute grand potential for a given phase, Ω^k is constructed by linking the relevant EE subensemble probability distribution, $\Pi_{EE}(\lambda)$ to the reference subensemble defined by $\lambda_r = (\xi_w, \xi_o, 0.0)$, for which the saturation condition is known from our previous study

$$\beta\Omega^k(\lambda) = \beta\Omega^k(\lambda_r) - \ln\left[\frac{\Pi_{EE}(\lambda)}{\Pi_{EE}(\lambda_r)}\right] \tag{3}$$

DOI: 10.1021/acs.langmuir.9b00393
Langmuir 2019, 35, 6540−6549

The initial estimated λ^g is unlikely to be accurate, that is, eqs 1 and 2 are unlikely to be satisfied for all subensembles. As a result, we now refine our estimate of the coexistence point for each subensemble by locating the λ values that satisfy these constraints. In practice, we identify the saturation point by modifying ξ_w and ξ_o at fixed ξ_a. We write the difference in the grand potential of phase k at a new estimate λ^n and the original estimate λ^g as

$$\Omega^k(\lambda^n) = \Omega^k(\lambda^g) + \Delta\Omega^k(\lambda^g \rightarrow \lambda^n) \quad (4)$$

Histogram reweighting expressions provided in ref 35 are used to evaluate $\Delta\Omega^k(\lambda^g \rightarrow \lambda^n)$. In cases where λ^g and λ^n differ significantly, the calculation is repeated with λ^n serving as the new λ^g in the next set of EE simulations. This iterative process continues until a converged solution λ^{sat} is obtained. Two to three iterations are typically required.

Interfacial Properties. We employ an interface potential-based approach[36−39] to study the wetting properties of the water−octane−acetic acid mixture at a silica surface. Detailed information related to this approach is available in earlier reports from our group.[33,34,40−49] We work with two variants of the interface potential. The water spreading interface potential, $W^{w,os}(l^w)$ provides the surface excess free energy associated with the growth of a water-rich film of thickness, l^w from the silica surface in a mother octane-rich liquid. The octane spreading interface potential, $W^{o,ws}(l^o)$ provides the surface excess free energy associated with the growth of an octane-rich film of thickness, l^o from the silica surface in a mother water-rich liquid. Examples of $W^{w,os}(l^w)$ and $W^{o,ws}(l^o)$ are provided in Figures 2 and 3, respectively, of ref 47. For partial wetting conditions, the water and octane spreading coefficients, $s^{w,os}$ and $s^{o,ws}$, are obtained from an analysis of the water and octane interface potentials, respectively. More specifically, $s^{w,os}$ and $s^{o,ws}$ are given by the difference in the minimum and plateau regions of the relevant interface potential. These spreading coefficients are used to determine the water−octane interfacial tension, $2\gamma^{ow} = -(s^{w,os} + s^{o,ws})$, and the contact angle θ of a water-rich droplet at a silica substrate in a mother octane-rich fluid, $2\gamma^{ow}\cos\theta = s^{w,os} - s^{o,ws}$.

A two-step approach is used to obtain γ^{ow} and θ over a wide range of state conditions and/or substrate characteristics. Detailed information is provided in a recent report from our group.[47] In the first step, direct calculations are conducted to compute $W^{w,os}(l^w)$ and $W^{o,ws}(l^o)$ curves at select conditions, from which we extract absolute values of $s^{w,os}$ and $s^{o,ws}$, respectively. Independent EE calculations are then used to determine how the free energies of the minimum and plateau regions of the interface potential vary along a path of interest. The results of these calculations are combined to obtain the variation in a spreading coefficient ($s^{w,os}$ or $s^{o,ws}$) along the path. Finally, the relative spreading coefficient curve is connected to a known absolute value of the spreading coefficient at a given point. Once $s^{w,os}$ and $s^{o,ws}$ are known along the path of interest, γ^{ow} and θ readily follow.

In our previous study,[47] we obtained $s^{w,os}$, $s^{o,ws}$, γ^{ow}, and θ over a wide range of temperatures and pressures at two values of the substrate polarity (see model details below). In this work, we are interested in how interfacial properties vary with acetic acid activity at fixed temperature, pressure, and substrate characteristics. We employ the EE framework outlined above to determine the variation in the wetting properties with acetic acid activity. We follow a path defined by a bulk saturation curve. Results from our previous study[47] provide the necessary $s^{w,os}$ and $s^{o,ws}$ reference data.

MOLECULAR MODEL

Model. We work with the SPC/E model[50] for water, the united atom TraPPE model for octane[51] and acetic acid,[52] and the Lee and Rossky[53] model for silica. The energy of interaction $u(r)$ between two interaction sites separated by four or more bonds and by a distance, r is given by the potential

$$u(r) = 4\varepsilon_{ij}\left[\left(\frac{\sigma_{ij}}{r}\right)^{12} - \left(\frac{\sigma_{ij}}{r}\right)^{6}\right]S(r) + \frac{1}{4\pi\varepsilon_o}\frac{q_i q_j}{r} \quad (5)$$

with

$$S(r) = \begin{cases} 1 & r < r_{c1} \\ \dfrac{(r_{c2}^2 - r^2)^2(2r^2 + r_{c2}^2 - 3r_{c1}^2)}{(r_{c2}^2 - r_{c1}^2)^3} & r_{c1} \le r \le r_{c2} \\ 0 & r > r_{c2} \end{cases} \quad (6)$$

where σ_{ij} and ε_{ij} are size and energy parameters, respectively, and q_i denotes the value of the partial charge placed at interaction site, i. The interaction parameters are provided in Table 1. Cross interaction parameters are computed using

Table 1. Potential Parameters for the Model Studied

model	atom	σ (Å)	ε (kJ mol^{-1})	q (e)
water[50]	O	3.166	0.650	−0.8476
	H	0	0	+0.4238
n-octane[51]	CH_3	3.75	0.815	0
	CH_2	3.95	0.383	0
acetic acid[52]	CH_3	3.75	0.815	+0.12
	C	3.90	0.341	+0.42
	O=(C)	3.05	0.657	−0.45
	O−(H)	3.02	0.773	−0.46
	H	0	0	+0.37
silica[53]	H	0	0	+0.40
	O	3.154	0.649	−0.71
	Si	3.795	0.534	+0.31

Lorentz−Berthelot combining rules.[54] $S(r)$ represents a switching function that brings the Lennard-Jones potential to zero between r_{c1} = 9.2 Å and r_{c2} = 10 Å. Long-range corrections for the Lennard-Jones potential are not included.

The water model is rigid. The intramolecular angle bending and torsion parameters for octane and acetic acid are taken from the TraPPE-UA[51] and OPLS-UA[52] force field. A harmonic potential is used to describe bond stretching within octane and acetic acid. The equilibrium bond length is taken from the TraPPE-UA force field[51,52] and the spring constant is adopted from the OPLS force field.[52,55] This modification was implemented to accommodate single-molecule hybrid MC moves[32] used to sample the intramolecular degrees of freedom of octane and acetic acid. Electrostatic interactions are calculated using the Ewald sum method.[54] For interfacial simulations, we implement the three-dimensional Ewald summation with a dipole correction term (EW3DC) as outlined by Yeh and Berkowitz.[56] Empty space extending 170 Å in the z direction is included between periodic images.

Simulation Details. Bulk simulations are completed in a cubic box (32 × 32 × 32 Å^3) with periodic boundary conditions applied in all directions. For direct GC simulations, the MC move mix includes 35% molecular displacements and rotations, 5% single-molecule hybrid MC moves,[32] and 60% molecular insertions (or growth) and deletions (or reductions). For EE simulations, the MC move mix includes 53% molecular displacements and rotations, 5% single-molecule hybrid MC moves (octane and acetic acid),[32] 40% molecular insertions (or growth) and deletions (or reductions), and 2% subensemble change moves.

Interfacial simulations are completed using a rectangular parallelepiped simulation box (L_x = 34.58 Å, L_y = 29.94 Å, L_z = 120 Å) with periodic boundary conditions applied in the x and

DOI: 10.1021/acs.langmuir.9b00393
Langmuir 2019, 35, 6540−6549

y directions. The system is closed at two ends of the nonperiodic z direction with the silica wall (34.58 × 29.94 × 14.95 Å) placed at the bottom of the box and a structureless "control" wall located at the other end. The substrate potential at the control wall is described by

$$u_{ci}(z) = \begin{cases} \infty & z \le 0 \\ \varepsilon_c S(z)\left[\left(\frac{\sigma_c}{z}\right)^9 + m_i\right] & 0 < z \le z_{c2} \\ 0 & z > z_{c2} \end{cases} \quad (7)$$

where z is the distance between a fluid interaction site and the wall. Here, the switching function, $S(z)$ brings the potential to zero between $z_{c1} = 0$ and $z_{c2} = 4\sigma_c$. For the water spreading method, we take m_i to be +1 for water, −1 for octane, and +1 for acetic acid, when constructing $W^{w,os}(l^w)$. In this case, the control wall is setup to be repulsive to water ($m_w = +1$) and acetic acid ($m_a = +1$), but attractive to octane ($m_o = -1$). For the octane spreading method, we take m_i to be −1 for water, +1 for octane, and +1 for acetic acid when constructing $W^{o,ws}(l^o)$. The control wall is then repulsive to octane ($m_o = +1$) and acetic acid ($m_a = +1$), but attractive to water ($m_w = -1$). We use potential parameters $\sigma_c = 4$ Å and $\varepsilon_c = 4.157$ kJ/mol.

We reproduce the hydroxylated β-cristobalite (111) surface following the work of Lee and Rossky.[53] For this silica model, partial charges are placed on oxygen, silicon, and hydrogen atoms closest to the fluid interface (first layer only). The substrate is electrostatically neutral. The surface charges are used to control the polarity of the substrate. Specifically, we scale the charge of the surface Si, O, and H atoms by a constant k, with $q_i = kq_i^o (0 \le k \le 1)$, i = Si, O, H, and q_i^o is the partial charge value for the standard silica surface. Therefore, $k = 1$ corresponds to the fully hydroxylated substrate and $k = 0$ maps to a nonpolar surface. Giovambattista et al.[57] characterize surfaces with $k < 0.4$ as hydrophobic and those with $k > 0.4$ as hydrophilic at $T = 300$ K.

For direct GC simulations, the MC move mix includes 35% molecular displacements and rotations, 5% single-molecule hybrid MC moves (octane and acetic acid),[32] 1% surface hydrogen rotation moves, and 59% molecular insertions (or growth) and deletions (or reductions). For EE simulations, the MC move mix includes 53% molecular displacements and rotations, 5% single-molecule hybrid MC moves (octane and acetic acid),[32] 1% surface hydrogen rotation moves, 39% molecular insertions (or growth) and deletions (or reductions), and 2% subensemble change moves.

Four sets of calculations are performed at liquid−liquid saturation conditions at $p = 10$ MPa. We consider wetting properties at a silica substrate characterized by $k = 0.4$ at temperatures of $T = 300$, 350, and 400 K. We also examine a system with a silica substrate with $k = 0.6$ at a temperature of $T = 400$ K. The bulk liquid−liquid saturation points for the binary octane−water mixture at temperatures of $T = 300$, 350, and 400 K are defined by activities ($\ln \chi$, η_o) of (−11.746, 0.964), (−10.092, 0.912), and (−8.923, 0.833), respectively.

Statistical uncertainties are determined by performing four independent sets of simulations. The standard deviation of the results from the four simulation sets are taken as an estimate of the statistical uncertainty.

RESULTS AND DISCUSSION

Pure Acetic Acid. We first examine the saturation properties of pure acetic acid. Saturated density and vapor pressure data for acetic acid are provided in Figures 1 and 2,

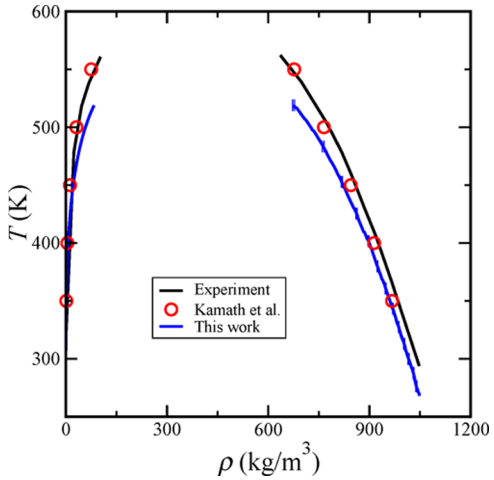

Figure 1. Saturated densities for acetic acid. Experimental data[58] and previous simulation results[52] are shown as black lines and red circles, respectively.

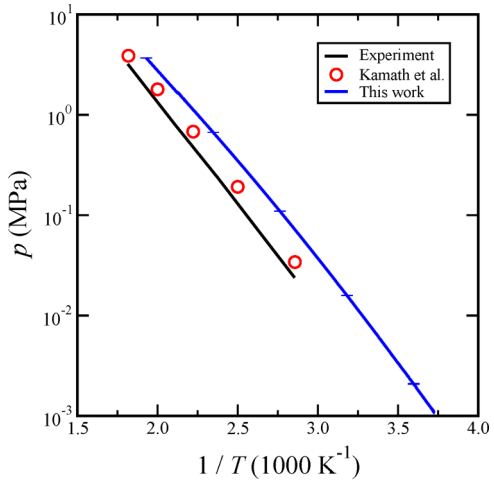

Figure 2. Vapor pressure against inverse temperature for acetic acid. Experimental data[58] and previous simulation results[52] are shown as black lines and red circles, respectively.

respectively. These figures contain experimental data,[58] simulation results for the TraPPE-UA model from the work of Kamath et al.,[52] and results for the TraPPE-UA model from this study. We note that different schemes to truncate the Lennard-Jones interaction are employed in the two simulation studies. Kamath et al. considered the full potential. In contrast, we use the switching potential noted above to truncate the potential. We adopted this approach to be consistent with our previous studies focused on the water−octane−silica system[47] and those strategies commonly employed by the simulation community for interfacial systems.[53,59−61] It is observed that the saturated liquid(vapor) densities of the truncated model are consistently under(over)estimated. The comparison shows that the truncated model overestimates the vapor pressure by approximately a factor of 2.4. In contrast, the full model overestimates the vapor pressure by approximately a factor of

DOI: 10.1021/acs.langmuir.9b00393
Langmuir 2019, 35, 6540−6549

1.4. The same qualitative trends were observed for *n*-octane in our previous study.[35] In short, truncation of the dispersion interaction leads to a decrease in the critical temperature and pressure, a decrease in saturated liquid densities, and an increase in vapor pressures.

Mixture Saturation Properties. In this section, activity fraction EE simulations are used to obtain liquid−liquid phase coexistence data of the octane−water−acetic acid ternary system at a pressure of p = 10 MPa and temperatures of T = 300, 350, and 400 K. In our previous work, we obtained the liquid−liquid saturation properties of the binary octane−water system at these conditions. For the ternary system at a given temperature, we use the binary mixture as a reference point and investigate how saturation properties vary within the range $\eta_a \in [0, 0.1]$. The objective is to establish the relationship ($\ln \chi$, η_o, η_a) along the saturation curve at fixed temperature and pressure.

We use a two-step process to determine the saturation properties. In the first step, we focus on the range of $\eta_a \in [0, 0.01]$. In this narrow range of η_a, the change in the composition is relatively small. To develop an initial estimate of the saturation curve, we assume that $\ln \chi$ and the ratio $\eta_w/\eta_o = \xi_w/\xi_o$ remain constant for the narrow range of η_a examined. Activity fraction EE simulations are then completed to compute the grand potential of the octane-rich phase and water-rich phase over the aforementioned η_a range. We produce a new estimate of the saturation activities at each activity fraction by employing the algorithm outlined in the Methods section. We next construct an estimate of the saturation conditions for the full range $\eta_a \in [0, 0.1]$ via extrapolation. The iterative procedure described in the Methods section is again used to obtain the converged saturation curve.

Figure 3 provides shifts in activities as acetic acid is introduced to the system at T = 400 K and p = 10 MPa. These

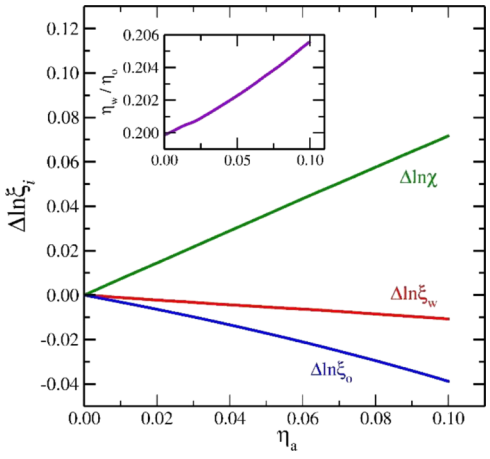

Figure 3. Evolution of saturated activities with acetic acid activity fraction. The green, red, and blue curves represent the sum of the activities, water activity, and octane activity, respectively. The inset provides the evolution of the ratio of the water and octane activity fractions along the same path.

shifts are characterized by $\Delta X(\eta_a) = X(\eta_a) - X(\eta_a = 0)$. The shifts in $\ln \xi_o$ and $\ln \xi_w$ are small relative to the shift in $\ln \chi$. We also observe that the change in $\ln \xi_o$ is a factor of four larger than that for $\ln \xi_w$. Recall that we assumed that $\ln \chi$ and η_w/η_o remain constant to generate an initial estimate of the saturated activities ($\eta_a \in [0, 0.01]$ range). The first assumption is not supported by the data, as $\ln \chi$ increases considerably over the range of η_a considered. The second assumption is supported by the data, as the ratio η_w/η_o increases by less than 3% over the $\eta_a \in [0, 0.1]$ range (see inset to Figure 3). In retrospect, it would have been preferable to assume that $\ln \xi_o$ and $\ln \xi_w$ remain constant upon variation of η_a. In the second step of the process ($\eta_a \in [0, 0.1]$ range), we assumed $\ln \xi_w$, $\ln \xi_o$, and $\ln \chi$ vary linearly with η_a. This approach is supported by the data, as the relationships for $\Delta \ln \xi_w$, $\Delta \ln \xi_o$, and $\Delta \ln \chi$ with η_a are nearly linear.

Figure 4 shows the mass fraction of acetic acid, w_a^k in the water-rich and octane-rich phases as a function of the acetic

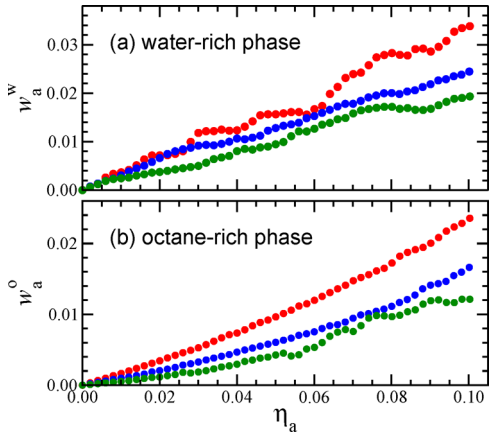

Figure 4. Mass fraction of acetic in (a) water-rich phase and (b) octane-rich phase at 300 K (green), 350 K (blue), and 400 K (red). Average uncertainties are 16 and 6% for the water-rich and octane-rich phases, respectively. Note that the "wiggles" in the curves are not statistically relevant.

acid activity fraction at temperatures of T = 300, 350, and 400 K. The solubilities vary nearly linearly with η_a. The acetic acid solubilities remain relatively modest over the range of η_a considered, with the mass fraction not exceeding 4% in the water-rich phase and 3% in the octane-rich phase. The mass fraction of acetic acid in the water-rich phase is approximately 40% higher than that in the octane-rich phase. The solubility of acetic acid increases with increasing temperature for both phases, with the solubility increasing by approximately a factor of two from 300 to 400 K.

Interfacial Properties. Now, we turn our attention to the wetting properties of the ternary mixture. Our primary goal is to compute the liquid−liquid wetting behavior along the three bulk saturation lines discussed above (T = 300, 350, and 400 K). We work with silica surfaces characterized by substrate polarities of k = 0.4 and 0.6. The wetting properties of the binary octane−water mixture at these silica surfaces were obtained in a previous study.[47] The water and octane spreading coefficient, water contact angle, and liquid−liquid interfacial tension at these conditions are collected in Table 2. The surface characterized by k = 0.4 is oil-wet, and the k = 0.6 case corresponds to a neutral wetting scenario. The composition-dependence of these interfacial properties is captured here with the activity fraction EE approach outlined above.

We begin by considering the fluid structure. Figure 5 provides data from an activity fraction EE simulation focused on the plateau region of the water spreading potential at T = 400 K with the k = 0.4 silica substrate. Within these

DOI: 10.1021/acs.langmuir.9b00393
Langmuir 2019, 35, 6540−6549

Table 2. Interfacial Properties of the Water−Octane−Silica System

T (K)	k	$s^{w,os}$ (mN/m)	$s^{o,ws}$ (mN/m)	γ^{ow} (mN/m)	θ (deg)
300	0.4	−90(1)	−28(2)	59(1)	122(2)
350	0.4	−78(1)	−24(2)	51(1)	122(2)
400	0.4	−64(1)	−18(1)	41(1)	124(2)
400	0.6	−40(1)	−44(1)	41(1)	88(2)

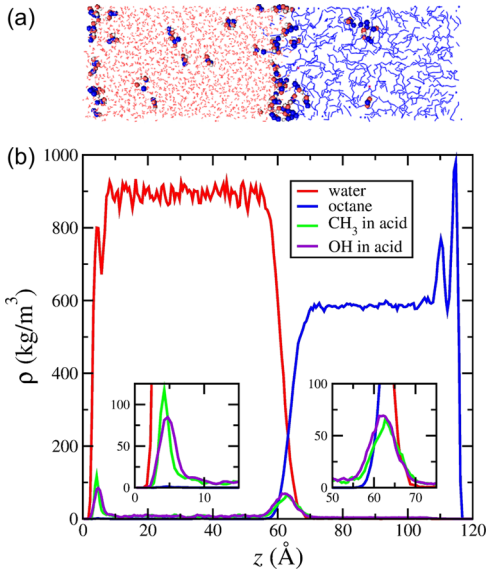

Figure 5. Snapshot of the water−octane−acetic acid mixture. (b) Representative density profiles within the plateau region of the water spreading interface potential with the k = 0.4 substrate at 400 K and η_a = 0.09.

simulations, an aqueous film resides between the silica substrate and an octane-rich film. The octane-rich film is also constrained by a control wall at the opposite end of the simulation box. We examine the structure for the subensemble characterized by η_a = 0.09. A snapshot of the water−octane−acetic acid mixture is shown in Figure 5a. To enhance clarity, acetic acid molecules are drawn in spacefill format, whereas water and octane and drawn as wireframe format. The snapshot suggests that acetic acid tends to accumulate at the water−octane and water−silica interfaces. This visual observation is supported by the density profiles provided in Figure 5b. Here, we show the mass density of the three components as a function of the distance, z from the top layer of oxygen atoms within the silica substrate. The acetic acid density is clearly enhanced at the water−octane and silica−water interfaces. The peak associated with the water−octane interface has a lower amplitude and broader span than that for the silica−water interface. The density profile for the CH_3 functional group within acetic acid at the water−octane interface is shifted slightly toward the octane-rich phase relative to that for the OH functional group. This shift suggests that the CH_3 group orients toward the octane-rich phase, whereas the OH group orients toward the water-rich phase. There is a slight shift of the CH_3 profile at the silica−water interface toward the relatively hydrophobic k = 0.4 substrate relative to the OH profile.

Figure 6 provides analogous structural data from an activity fraction EE simulation focused on the plateau region of the octane spreading potential at T = 400 K and η_a = 0.09 with the

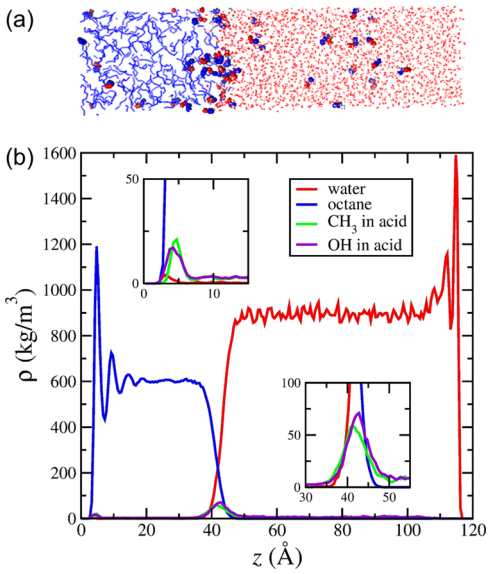

Figure 6. Snapshot of the water−octane−acetic acid mixture. (b) Representative density profiles within the plateau region of the octane spreading interface potential with the k = 0.4 substrate at 400 K and η_a = 0.09.

k = 0.4 silica substrate. Within these simulations, an octane film resides between the silica substrate and a water-rich film. The water-rich film is also constrained by a control wall. A snapshot of the water−octane−acetic acid mixture is shown in Figure 6a and mass density profiles are provided in Figure 6b. We again find that acetic acid accumulates at the water−octane interface. The data also indicate that acetic acid has a slight preference for the silica−octane interface. The amplitude of the CH_3 and OH profiles near the silica substrate are approximately a factor of four lower than those for the water spreading case (Figure 5). In contrast to the water spreading case, the OH profile is shifted slightly toward the substrate relative to the CH_3 profile.

Figure 7 shows the average number of acetic acid molecules adsorbed at each interface for systems at T = 400 K with k =

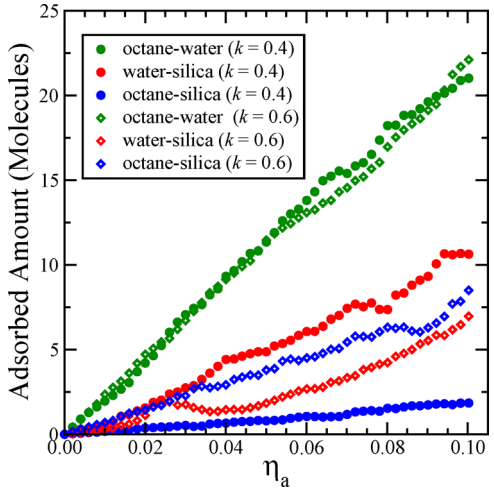

Figure 7. The amount of acetic acid adsorbed at the octane−water, water−silica, and octane−silica interfaces. Average uncertainties for the octane−water, water−silica, and octane−silica data are 7, 15, and 11, respectively. Note that the "wiggles" in the curves are not statistically relevant.

DOI: 10.1021/acs.langmuir.9b00393
Langmuir 2019, 35, 6540−6549

0.4 and 0.6 substrates. As shown in Figures 5 and 6, we have three different interfaces. In the water spreading approach, the water-rich phase is in contact with silica and octane-rich phases, and therefore, we have water−silica and octane−water interfaces. In the octane spreading approach, the octane-rich phase is in contact with silica and the water-rich phase, and therefore, we have octane−silica and octane−water interfaces. Acetic acid shows the strongest preference for the water−octane interface. The average number of molecules adsorbed at this interface is more than twice that adsorbed at any of the silica−fluid interfaces. As expected, the adsorption density at the water−octane interface is independent of substrate polarity. Capturing data for both substrates simply provides a consistency check. The amount of acetic acid adsorbed at the silica−octane interface increases with an increase in substrate polarity. This result seems reasonable, as the increase in substrate polarity increases the driving force for the formation of hydrogen bonds between the substrate and acetic acid. In contrast, the amount of acetic acid adsorbed at the silica−water interface decreases with an increase in substrate polarity. This interesting trend is perhaps somewhat counterintuitive. The data suggest that the increase in substrate polarity results in a strengthening of the silica−water interaction relative to the silica−acetic acid interaction, thereby leading to a reduction in the amount of acetic acid adsorbed at the silica substrate. In other words, water displaces acetic acid at the silica−water interface as the substrate polarity increases.

Figure 8 provides data that illustrate the impact of temperature on the adsorption of acetic acid at the various interfaces. Acetic acid shows the strongest preference for the water−octane interface at all temperatures, and the amount of acid adsorbed at this interface decreases with increasing temperature. Interestingly, the amount of acetic acid adsorbed at the water−silica interface increases with increasing temperature, whereas the amount of acetic acid at the octane−silica interface decreases with increasing temperature. It appears that the strength of the silica−acetic acid interaction strengthens relative to the silica−water interaction with an increase in temperature. As a result, acetic acid displaces water at the silica−water interface as the temperature increases. In contrast, the strength of the silica−acetic acid interaction weakens relative to the silica−octane interaction with an increase in temperature. Octane displaces acetic acid at the silica−octane interface as the temperature increases.

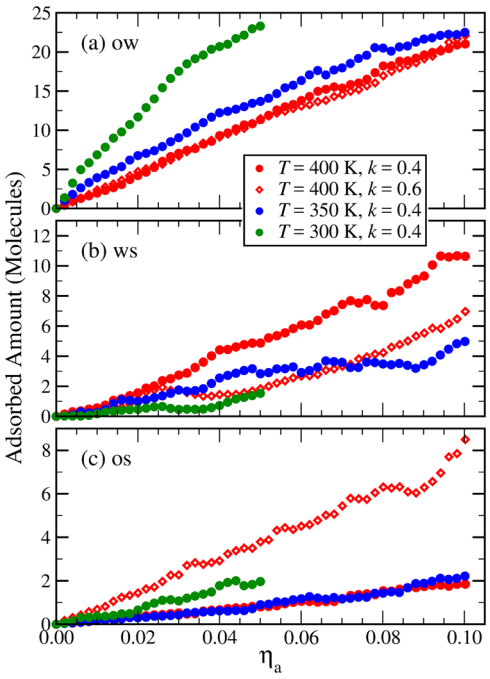

Figure 8. The amount of acetic acid adsorbed at the (a) octane−water, (b) water−silica, and (c) octane−silica interfaces. Average uncertainties for the octane−water, water−silica, and octane−silica data are 6, 18, and 15%, respectively. Note that the "wiggles" in the curves are not statistically relevant.

We now consider the shift in thermodynamic properties upon introduction of acetic acid to the water−octane−silica system. Figure 9 provides the change in the spreading

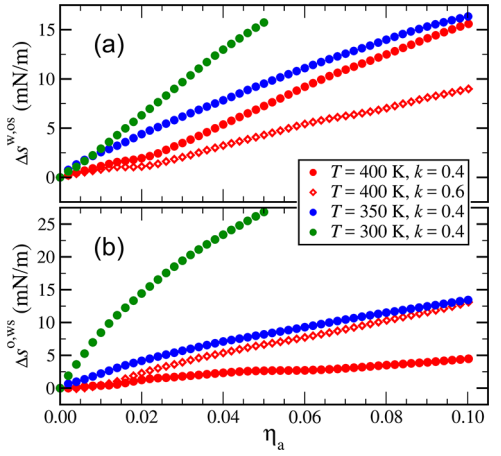

Figure 9. The evolution of (a) water spreading coefficient and (b) octane spreading coefficient with the activity fraction of acetic acid. Average uncertainties for the water and octane spreading coefficients are 0.8 and 1.7 mN/m, respectively.

coefficients, $s^{w,os}$ and $s^{o,ws}$ upon variation of η_a. Both $s^{w,os}$ and $s^{o,ws}$ increase with increasing η_a. Given that $s^{w,os} < 0$ and $s^{o,ws} < 0$ within the partial wetting regime, this result indicates that the magnitudes of the spreading coefficients decrease upon the addition of acetic acid to the system. We truncate the $T = 300$ K and $k = 0.4$ data at $\eta_a \approx 0.05$ because it is at this point that $s^{o,ws}$ goes to zero. The shifts in $s^{w,os}$ and $s^{o,ws}$ closely align with the amount of acetic acid that adsorbs at the silica−fluid interface. For example, in the $T = 400$ K and $k = 0.4$ case, $s^{w,os}$ increases at a rate that is approximately a factor of three larger than that for $s^{o,ws}$. This shift mirrors the adsorption data provided in Figure 7, wherein the amount of acid that adsorbs at the water−silica interface is approximately a factor of three higher than that for the silica−octane interface.

The octane−water interfacial tension is defined by $2\gamma^{ow} = -(s^{w,os} + s^{o,ws})$, and the water contact angle is defined by $\cos\theta = -(s^{w,os} - s^{o,ws})/(s^{w,os} + s^{o,ws})$. Figure 10 provides the shifts in the combinations $s^{w,os} + s^{o,ws}$ and $s^{w,os} - s^{o,ws}$ upon variation of η_a. Given that $s^{w,os}$ and $s^{o,ws}$ both increase with η_a in all cases, it readily follows that the combination $s^{w,os} + s^{o,ws}$ also increases with increasing η_a. In the $T = 400$ K and $k = 0.6$ case, $s^{o,ws}$ increases at a slightly faster rate than $s^{w,os}$, which results in a decrease in $s^{w,os} - s^{o,ws}$ and a shift in the system toward the octane-wet case. The evolution of $s^{w,os} - s^{o,ws}$ with η_a for the $k = 0.4$ substrate varies qualitatively with temperature. At 400 K, $s^{w,os} - s^{o,ws}$ increases upon increasing η_a, suggesting a shift toward the water-wet state. In contrast, $s^{w,os} - s^{o,ws}$ decreases

DOI: 10.1021/acs.langmuir.9b00393
Langmuir 2019, 35, 6540−6549

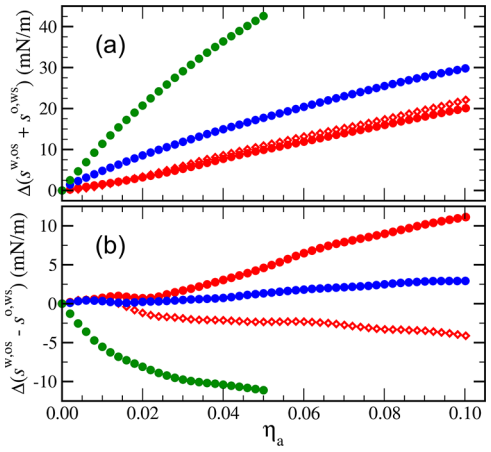

Figure 10. The evolution of (a) sum and (b) difference in the water and octane spreading coefficients with the activity fraction of acetic acid. Symbols are defined in the same manner as in Figure 9. The average uncertainty for the sum and difference in the water and octane spreading coefficients is 1.9 mN/m.

significantly upon increasing η_a at 300 K, suggesting a shift toward the octane-wet state.

Figure 11 provides the response of γ^{ow} and cos θ upon variation of η_a. In all cases, γ^{ow} decreases in a near linear

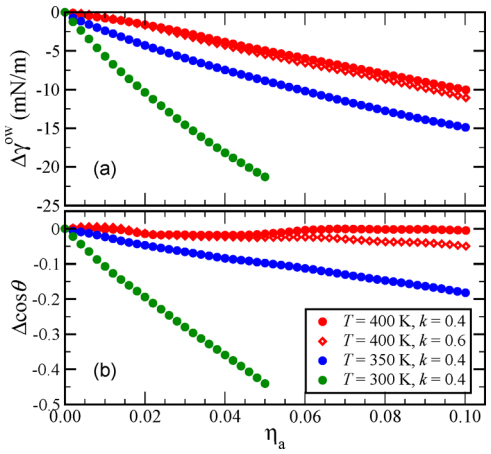

Figure 11. The evolution of (a) octane–water interfacial tension and (b) cosine of the contact angle with the activity fraction of acetic acid. Average uncertainties for the interfacial tension and cosine of the contact angle are 0.9 mN/m and 0.029, respectively.

manner upon increasing η_a. The response of γ^{ow} upon variation of η_a indicates that acetic acid acts as a surfactant at the water–octane interface. Modest bulk concentrations of acetic acid lead to a significant reduction in γ^{ow}. The analysis for cos θ is a bit more complex. For T = 400 K and k = 0.6, the change in $s^{w,os} - s^{o,ws}$ is relatively small and there is relatively little change in cos θ. For T = 400 K and k = 0.4, there is a moderate increase in $s^{w,os} - s^{o,ws}$ that directs the system toward the water-wet case, but this change is offset by an increase in $s^{w,os} + s^{o,ws}$. As a result, cos θ remains relatively constant with η_a. For T = 350 K and k = 0.4, there is a relatively small increase in $s^{w,os} - s^{o,ws}$ and a relatively large increase $s^{w,os} + s^{o,ws}$ (decrease in γ^{ow}). The combination produces an increase in the water contact angle. Finally, for T = 300 K and k = 0.4, both $s^{w,os} - s^{o,ws}$ and $s^{w,os} + s^{o,ws}$ evolve in a manner that favors an increase in the contact angle. The end result is a relatively rapid change in cos θ with the system reaching a complete octane wetting condition at $\eta_a \approx 0.05$. The shift in the contact angle is qualitatively consistent with results from the experimental study of Wu et al.[18] This group considered the contact angle of water on calcite surfaces treated with various naphthenic acids. In all cases, they observed that the presence of a naphthenic acid resulted in an increase in the water contact angle.

We next explore the connection between the interfacial tension and the adsorption of acetic acid at the water–octane interface. Figure 12 provides the change in γ^{ow} with N_a^{ow} at

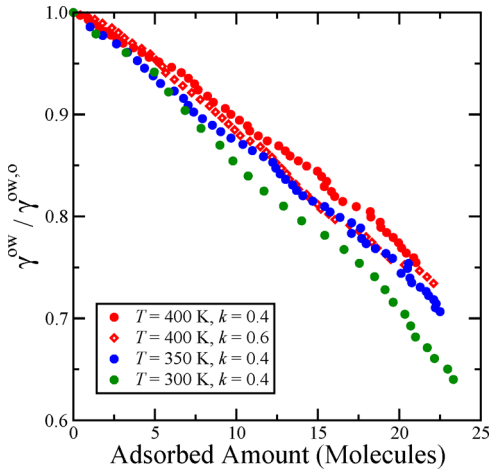

Figure 12. The evolution of normalized octane–water interfacial tension with the quantity of acetic acid that adsorbs at the interface.

temperatures of 300, 350, and 400 K. The γ^{ow} data are normalized by the temperature-specific interfacial tension of the octane–water case, $\gamma^{ow,o} = \gamma^{ow}(\eta_a = 0)$. From a quantitative perspective, γ^{ow} is reduced by 25–35% over the range of η_a shown. In all cases, the interfacial tension decreases in a near-linear manner with the number of acetic acid molecules adsorbed at the interface. The influence of temperature also appears to be relatively small, with the three curves nearly collapsed. The linear nature of the γ^{ow} with N_a^{ow} curves suggests that acetic acid molecules effectively act independently at the water–octane interface. At sufficiently high η_a, one would expect the density of acetic acid to increase to a level wherein the acetic acid molecules act in a cooperative manner. It would be interesting to examine this regime in a subsequent study.

CONCLUSIONS

We employed MC simulation to study the variation of wetting properties of a model water–octane–silica system upon the addition of a polar organic molecule, acetic acid. The saturation properties of the bulk fluid were computed first. We evaluated the liquid–vapor properties of acetic acid over a broad range of temperatures. We then collected the liquid–liquid saturation properties of the ternary water–octane–acetic acid mixture over a broad range of acetic acid activities at constant temperature and pressure. An interface potential approach was then used to determine the response of the octane–water interfacial tension and water contact angle upon the addition of acetic acid to the water–octane–silica system. Multiple temperatures and substrate polarities were considered.

For the bulk ternary mixture, acetic acid distributes relatively evenly (mass fraction) between the two coexisting liquid

DOI: 10.1021/acs.langmuir.9b00393
Langmuir 2019, 35, 6540–6549

phases, with a slight preference for the water-rich phase. When acetic acid is added to the water−octane−silica interfacial system, it preferentially resides at the octane−water and silica−fluid interfaces. The level of adsorption at silica−fluid interfaces varies considerably with the hydrophilicity of the substrate. In all cases, the water and octane spreading coefficients increase (decrease in magnitude) with the introduction of acetic acid. It follows that the interfacial tension decreases with increasing acetic acid activity. Acetic acid acts as a surfactant, producing a 25−35% decrease in the interfacial tension over the range of conditions considered here. The shift in the contact angle varied with temperature and substrate polarity, suggesting that the response of the contact angle depends sensitively on substrate conditions.

There are several ways that one could extend this research. Acetic acid represents just one of many polar organic compounds typically found within crude oil. Salts and other molecules not considered here are also present in oil and are known to influence wetting properties. Likewise, there are a number of minerals and their various crystallographic faces that form the surfaces of rocks. In principle, all of these factors could be explored via molecular simulation using the methods described here. Developing a better fundamental understanding of the connections between reservoir state conditions (e.g., temperature, pressure), the chemical features of polar organic molecules, solution conditions, the characteristics of mineral surfaces, and the wetting behavior of a system would prove advantageous in the design of EOR strategies. Various modeling strategies (e.g., force fields) could be employed to study rock−brine−oil systems. Exploring the sensitivity of wetting properties to model selection would also prove beneficial.

AUTHOR INFORMATION

Corresponding Author

*E-mail: jerring@buffalo.edu. Phone: +1 (716) 645-1184.

ORCID

Jeffrey R. Errington: 0000-0003-0365-0271

Notes

The authors declare no competing financial interest.

ACKNOWLEDGMENTS

We gratefully acknowledge the financial support of the National Science Foundation (grant no. CBET-1705620). Computational resources were provided in part by the University at Buffalo Center for Computational Research.

REFERENCES

(1) Morrow, N. R. Wettability and its effect on oil recovery. *J. Petrol. Technol.* **1990**, *42*, 1476−1484.

(2) Roehl, P. O.; Choquette, P. W. *Carbonate Petroleum Reservoirs*; Springer-Verlag: New York, 1985.

(3) Austad, T.; Standnes, D. C. Spontaneous imbibition of water into oil-wet carbonates. *J. Pept. Sci. Eng.* **2003**, *39*, 363−376.

(4) Zhong, J.; Wang, P.; Zhang, Y.; Yan, Y.; Hu, S.; Zhang, J. Adsorption mechanism of oil components on water-wet mineral surface: A molecular dynamics simulation study. *Energy* **2013**, *59*, 295−300.

(5) Wagner, O. R.; Leach, R. O. Improving oil displacement efficiency by wettability adjustment. *Trans. AIME* **1959**, *216*, 65.

(6) Zheng, J.; Powers, S. E. Organic bases in NAPLs and their impact on wettability. *J. Contam. Hydrol.* **1999**, *39*, 161−181.

(7) Alipour Tabrizy, V.; Denoyel, R.; Hamouda, A. A. Characterization of wettability alteration of calcite, quartz and kaolinite: Surface energy analysis. *Colloids Surf., A* **2011**, *384*, 98−108.

(8) Fathi, S. J.; Austad, T.; Strand, S.; Puntervold, T. Wettability alteration in carbonates: The effect of water-soluble carboxylic acids in crude oil. *Energy Fuels* **2010**, *24*, 2974−2979.

(9) Chernicoff, S. *Geology*, 2nd ed.; Houghton Mifflin Company: Boston, 1999.

(10) Salehi, M.; Johnson, S. J.; Liang, J.-T. Mechanistic study of wettability alteration using surfactants with applications in naturally fractured reservoirs. *Langmuir* **2008**, *24*, 14099−14107.

(11) Hammond, P. S.; Unsal, E. Spontaneous and forced imbibition of aqueous wettability altering surfactant solution into an initially oil-wet capillary. *Langmuir* **2009**, *25*, 12591−12603.

(12) Hammond, P. S.; Unsal, E. Forced and spontaneous imbibition of surfactant solution into an oil-wet capillary: The effects of surfactant diffusion ahead of the advancing meniscus. *Langmuir* **2010**, *26*, 6206−6221.

(13) Thomas, M. M.; Clouse, J. A.; Longo, J. M. Adsorption of organic compounds on carbonate minerals. *Chem. Geol.* **1993**, *109*, 201−213.

(14) Standnes, D. C.; Austad, T. Wettability alteration in chalk. *J. Pept. Sci. Eng.* **2000**, *28*, 111−121.

(15) Standnes, D. C.; Austad, T. Wettability alteration in chalk. *J. Pept. Sci. Eng.* **2000**, *28*, 123−143.

(16) Hansen, G.; Hamouda, A. A.; Denoyel, R. The effect of pressure on contact angles and wettability in the mica/water/n-decane system and the calcite+stearic acid/water/n-decane system. *Colloids Surf., A* **2000**, *172*, 7−16.

(17) Rezaei Gomari, K. A.; Hamouda, A. A. Effect of fatty acids, water composition and pH on the wettability alteration of calcite surface. *J. Pept. Sci. Eng.* **2006**, *50*, 140−150.

(18) Wu, Y.; Shuler, P. J.; Blanco, M.; Tang, Y.; Goddard, W. A. An experimental study of wetting behavior and surfactant EOR in carbonates with model compounds. *SPE Journal* **2008**, *13*, 26−34.

(19) Shariatpanahi, S. F.; Strand, S.; Austad, T. Evaluation of water-based enhanced oil recovery (EOR) by wettability alteration in a low-permeable fractured limestone oil reservoir. *Energy Fuels* **2010**, *24*, 5997−6008.

(20) Cooper, T. G.; de Leeuw, N. H. A computer modeling study of the competitive adsorption of water and organic surfactants at surfaces of the mineral Scheelite. *Langmuir* **2004**, *20*, 3984−3994.

(21) Shen, Y.; Couzis, A.; Koplik, J.; Maldarelli, C.; Tomassone, M. S. Molecular dynamics study of the influence of surfactant structure on surfactant-facilitated spreading of droplets on solid surfaces. *Langmuir* **2005**, *21*, 12160−12170.

(22) Kvamme, B.; Kuznetsova, T.; Uppstad, D. Modelling excess surface energy in dry and wetted calcite systems. *J. Math. Chem.* **2009**, *46*, 756−762.

(23) Headen, T. F.; Boek, E. S. Potential of Mean Force Calculation from Molecular Dynamics Simulation of Asphaltene Molecules on a Calcite Surface†. *Energy Fuels* **2011**, *25*, 499−502.

(24) Jiménez-Ángeles, F.; Firoozabadi, A. Tunable substrate wettability by thin water layer. *J. Phys. Chem. C* **2016**, *120*, 24688−24696.

(25) Jiménez-Ángeles, F.; Firoozabadi, A. Contact Angle, Liquid Film, and Liquid-Liquid and Liquid-Solid Interfaces in Model Oil-Brine-Substrate Systems. *J. Phys. Chem. C* **2016**, *120*, 11910−11917.

(26) Jiang, H.; Müller-Plathe, F.; Panagiotopoulos, A. Z. Contact angles from Young's equation in molecular dynamics simulations. *J. Chem. Phys.* **2017**, *147*, 084708.

(27) Leroy, F.; dos Santos, D. J. V. A.; Müller-Plathe, F. Interfacial Excess Free Energies of Solid-Liquid Interfaces by Molecular Dynamics Simulation and Thermodynamic Integration. *Macromol. Rapid Commun.* **2009**, *30*, 864−870.

(28) Leroy, F.; Müller-Plathe, F. Solid-liquid surface free energy of Lennard-Jones liquid on smooth and rough surfaces computed by molecular dynamics using the phantom-wall method. *J. Chem. Phys.* **2010**, *133*, 044110.

DOI: 10.1021/acs.langmuir.9b00393
Langmuir 2019, 35, 6540−6549

(29) Holte, L. K.; Kuran, B. A.; Richmond, G. L.; Johnson, K. E. Computational Modeling of Lauric Acid at the Organic-Water Interface. *J. Phys. Chem. C* **2014**, *118*, 10024−10032.
(30) Riccardi, E.; Kovalchuk, K.; Mehandzhiyski, A. Y.; Grimes, B. A. Structure and Orientation of Tetracarboxylic Acids at Oil-Water Interfaces. *J. Dispersion Sci. Technol.* **2014**, *35*, 1018−1030.
(31) Tikhonov, A. M.; Patel, H.; Garde, S.; Schlossman, M. L. Tail Ordering Due to Headgroup Hydrogen Bonding Interactions in Surfactant Monolayers at the Water−Oil Interface. *J. Phys. Chem. B* **2006**, *110*, 19093−19096.
(32) Rane, K. S.; Murali, S.; Errington, J. R. Monte carlo simulation methods for computing liquid-vapor saturation properties of model systems. *J. Chem. Theory Comput.* **2013**, *9*, 2552−2566.
(33) Kumar, V.; Errington, J. R. Monte Carlo simulation strategies to compute interfacial and bulk properties of binary fluid mixtures. *J. Chem. Phys.* **2013**, *138*, 174112.
(34) Kumar, V.; Errington, J. R. Understanding wetting of immiscible liquids near a solid surface using molecular simulation. *J. Chem. Phys.* **2013**, *139*, 064110.
(35) Guo, W.; Bali, P.; Errington, J. R. Calculation of the Saturation Properties of a Model Octane-Water System Using Monte Carlo Simulation. *J. Phys. Chem. B* **2018**, *122*, 6260−6271.
(36) de Gennes, P. G. Wetting: statics and dynamics. *Rev. Mod. Phys.* **1985**, *57*, 827−863.
(37) Evans, R. *Liquids at Interfaces*; Elsevier: Amsterdam, 1990.
(38) Dietrich, S. *Phase Transitions and Critical Phenomena*; Academic Press: London, 1988.
(39) Indekeu, J. O. Line tension at wetting. *Int. J. Mod. Phys. B* **1994**, *08*, 309−345.
(40) Kumar, V.; Errington, J. R. Impact of small-scale geometric roughness on wetting behavior. *Langmuir* **2013**, *29*, 11815−11820.
(41) Kumar, V.; Errington, J. R. Wetting behavior of water near nonpolar surfaces. *J. Phys. Chem. C* **2013**, *117*, 23017−23026.
(42) Kumar, V.; Sridhar, S.; Errington, J. R. Monte Carlo simulation strategies for computing the wetting properties of fluids at geometrically rough surfaces. *J. Chem. Phys.* **2011**, *135*, 184702.
(43) Grzelak, E. M.; Errington, J. R. Calculation of interfacial properties via free-energy-based molecular simulation: The influence of system size. *J. Chem. Phys.* **2010**, *132*, 224702.
(44) Grzelak, E. M.; Errington, J. R. Computation of interfacial properties via grand canonical transition matrix Monte Carlo simulation. *J. Chem. Phys.* **2008**, *128*, 014710.
(45) Grzelak, E. M.; Errington, J. R. Nanoscale Limit to the Applicability of Wenzel's Equation. *Langmuir* **2010**, *26*, 13297−13304.
(46) Grzelak, E. M.; Shen, V. K.; Errington, J. R. Molecular simulation study of anisotropic wetting. *Langmuir* **2010**, *26*, 8274−8281.
(47) Guo, W.; Errington, J. R. Monte Carlo Simulation Strategies to Compute the Interfacial Properties of a Model Octane-Water-Silica System. *J. Phys. Chem. C* **2018**, *122*, 17309−17318.
(48) Sellers, M. S.; Errington, J. R. Influence of substrate strength on wetting behavior. *J. Phys. Chem. C* **2008**, *112*, 12905−12913.
(49) Rane, K. S.; Errington, J. R. Understanding the influence of Coulomb and dispersion interactions on the wetting behavior of ionic liquids. *J. Chem. Phys.* **2014**, *141*, 174706.
(50) Berendsen, H. J. C.; Grigera, J. R.; Straatsma, T. P. The missing term in effective pair potentials. *J. Phys. Chem.* **1987**, *91*, 6269−6271.
(51) Martin, M. G.; Siepmann, J. I. Transferable Potentials for Phase Equilibria. 1. United-Atom Description ofn-Alkanes. *J. Phys. Chem. B* **1998**, *102*, 2569−2577.
(52) Kamath, G.; Cao, F.; Potoff, J. J. An Improved Force Field for the Prediction of the Vapor−Liquid Equilibria for Carboxylic Acids. *J. Phys. Chem. B* **2004**, *108*, 14130−14136.
(53) Lee, S. H.; Rossky, P. J. A comparison of the structure and dynamics of liquid water at hydrophobic and hydrophilic surfaces-a molecular dynamics simulation study. *J. Chem. Phys.* **1994**, *100*, 3334−3345.
(54) Allen, M. P.; Tildesley, D. *Computer Simulation of Liquids*; Clarendon Press: Oxford, U.K., 1989.
(55) Damm, W.; Frontera, A.; Tirado-Rives, J.; Jorgensen, W. L. OPLS all-atom force field for carbohydrates. *J. Comput. Chem.* **1997**, *18*, 1955−1970.
(56) Yeh, I.-C.; Berkowitz, M. L. Ewald summation for systems with slab geometry. *J. Chem. Phys.* **1999**, *111*, 3155−3162.
(57) Giovambattista, N.; Debenedetti, P. G.; Rossky, P. J. Effect of surface polarity on water contact angle and interfacial hydration structure. *J. Phys. Chem. B* **2007**, *111*, 9581−9587.
(58) Vargaftik, N. B. *Handbook of Physical Properties of Liquids and Gases: Pure Substances and Mixtures*; Hemisphere Publishing Corporation, 1983.
(59) Feller, S. E.; Pastor, R. W.; Rojnuckarin, A.; Bogusz, S.; Brooks, B. R. Effect of electrostatic force truncation on interfacial and transport properties of water. *J. Phys. Chem.* **1996**, *100*, 17011−17020.
(60) Lagüe, P.; Pastor, R. W.; Brooks, B. R. Pressure-Based Long-Range Correction for Lennard-Jones Interactions in Molecular Dynamics Simulations: Application to Alkanes and Interfaces. *J. Phys. Chem. B* **2004**, *108*, 363−368.
(61) Winter, N.; Vieceli, J.; Benjamin, I. Hydrogen-Bond Structure and Dynamics at the Interface between Water and Carboxylic Acid-Functionalized Self-Assembled Monolayers. *J. Phys. Chem. B* **2008**, *112*, 227−231.

DOI: 10.1021/acs.langmuir.9b00393
Langmuir 2019, 35, 6540−6549